MANCHESTER 1824
The University of Manchester

Measurement of The Elementary Charge Using Solid-State Circuitry

Third Year Individual Project – Final Report

May 2021

Mohammed Alotaibi

9976361

Supervisor: Matthew Halsall

School of Electrical and Electronic Engineering

Contents

Total word count: 6684

1. Introduction

"The fact that Science walks forward on two feet, namely theory and experiment, is nowhere better illustrated than in the two fields for slight contributions to which you have done me the great honour of awarding the Nobel Prize in Physics for the year 1923. Sometimes it is one foot that is put forward first, sometimes the other, but continuous progress is only made by the use of both—by theorizing and then testing, or by finding new relations in the process of experimenting and then bringing the theoretical foot up and pushing it on beyond, and so on in unending alterations." — Robert Andrews Millikan [1]

Robert A. Millikan was the first to measure the charge on an electron in his famous oil-drop experiment. He measured the charge by balancing the electric force, the gravitational force, and the viscous force of a charged oil drop and seeing the relationship between them to calculate the elementary charge [2]. The elementary charge (the charge on an electron), first discovered in 1909, has recently, as of 2019, been given an official, definitive value of exactly $1.602176634 \times 10^{-19}\ C$ [3], this constant value is used to define the Ampere scale and keeps the Ampere universally constant [4].

In the years following Robert A. Millikan's experiment, several attempts were made to measure the elementary charge with better accuracy using newer technology, with some implementations using purely solid-state devices. A recent article called the "Simple do-it-yourself experimental setup for electron charge q_e measurement" was published in 2018 by T. M. Mishonov and his collaborators from institutions located in Sofia, Bulgaria. This article managed to measure the charge of an electron to an accuracy of 13% and suggested methods to reach an accuracy of 1%, doing so using simple, cheap, solid-state components [5].

All areas of physics and engineering use physical constants such as Planck's constant, Boltzmann's constant, and the electron charge. The constant physical values are taught and given in high school and university courses without the intuition of how they can be measured. This project develops an understanding of the fundamental constants. It offers a means of measuring elementary charge constant without costly equipment; instead, it uses cheap printable circuit boards and widely available components.

The following sections in this paper theoretically build on T. M. Mishonov's design found in [5]. His design's main amplifying component, the ADA4898-2 operational amplifier, is tested against

alternative operational amplifiers using the LTSpiceXVII Spice simulation software. The simulator simulates the overall output with the different design sections' components replaced with various component selections; different gain implementations are tested and recorded and analysed in the later sections.

T. M. Mishonov uses Young Walter Shottky's theory of Shot noise to perform the measurement and calculations. The Schottky relation is given by

$$(I^2)_f = 2q_e\langle I\rangle \quad (1)$$

where $\langle I\rangle$ is the averaged current and $(I^2)_f$ The spectral density of current noise is discussed in [5] and used later in the report.

The objective is to identify the relevant sources of noise affecting the existing designs and figure out how to mitigate them as best as possible. The next step is to find cheap higher quality components capable of outperforming the ones used in existing designs, then designing a high-speed, low noise layout capable of maximizing only the Shot noise present in the circuit. The final step is to introduce software code capable of performing all the necessary calculations.

The paper begins with a noise analysis section that elaborates on noise sources and methods to calculate and prevent them. The following section provides the component simulations and their descriptive results; After that, the paper includes the layout design with justifications for the layout decisions, which leads to the section deriving the mathematical equations to achieve the desired result. The program pseudo-code capable of performing the calculations are in the final subsection of this paper. The Appendix sections include the Altium 21 circuit schematic and layout and the complete pseudo-code for the design.

2. Noise Analysis

Generally, engineers aim to eradicate all sources of noise in circuits and view them as undesirable; in this project, however, a single source of noise, namely "Shot noise", is isolated from all other sources of noise, amplified, and measured. This section discusses sources of noises present in every circuit and suggests methods for deterring them or otherwise calculating their effects, thus considering them in the equation development stage. The sources of noise explored in this section are the Shot noise, Johnson noise (thermal noise), Burst noise, Flicker noise (1/f noise), Avalanche noise, Amplifier noise, Parasitic impedances, and Electromagnetic interference.

2.1. Shot Noise

The Schottky relation, as seen in equation (1), has its revision in the appendix section of [5]; [6] gives a detailed derivation of the Shot noise phenomenon. Shot noise is the current noise generated in a circuit due to the finite quantum nature of the electron charge. Shot noise arises when an electron crosses a PN junction in a diode or a transistor; this crossing of an electron creates a small voltage spike for every electron that crosses the junction. The sum of the voltage spikes results in a stochastic current emanating from the diode.

When taken as an exact impulse function, such as that derived in [6], shot noise is a source of white noise [7], having a uniform frequency distribution in the Fourier domain. In reality, its energy would decrease as the frequency increases, but that consideration is beyond the scope of this report. The later sections detail how this fluctuating current is measured, amplified, filtered, and measured again using solid-state components. Then the two measurements taken will be used in solving the Shottky relation equation (1), which will result in the calculation of the electron charge.

2.2. Unconventional noise sources

There are plenty of noise sources to worry about when designing circuits; some noise sources used to be a problem in the past due to older integrated circuit technology; for other sources, easily accessible solutions mitigate them. The following sources of noise are among those that are easily mitigated or are no longer considered an issue due to advancement in technology.

Burst noise arises because of impurities found in silicon wafers when printing integrated circuits or simply impurities found in simple diodes and transistors. Lattice impurities create rogue energy levels, which can sometimes trap electron momentarily. Burst noise occurs when an electron gets trapped at a rogue energy level and then later gets released; this release creates a voltage "burst", hence the name. Burst noise is no longer a problem in current-day technology, and so it is not a design problem.

Avalanche noise and electromagnetic interference do not pose a significant problem in the design; Avalanche noise occurs in the breaking point of a PN junction; Zener diodes are a typical avalanche noise source. The circuit is not operating near the breaking point of any diode, and so there is no avalanche noise present. Electromagnetic interference would generally be an issue in circuits operating in rough environments. However, in this case, the circuit can be electromagnetically

screened during the measurement process by placing it in a faraday cage such as a refrigerator or a box covered in aluminium foil or ferrite sheets.

2.3. Conventional noise sources

Johnson noise (thermal noise) is the most significant cause of disturbances in the measurement; Johnson noise is a type of Brownian motion; it is the small voltage fluctuations created within a resistor due to its thermal energy. Its RMS voltage, measured in $V/Hz^{1/2}$, is given by

$$v_{noise}(rms) = \sqrt{4kTRB} \quad (2)$$

where k is the Boltzmann constant $1.38064852 \times 10^{-23}\ m^2\ kg\ s^{-2}\ K^{-1}$, T is the resistor's temperature in Kelvins, R is the resistor value in Ohms, and B is the bandwidth in Hertz. The literature categorizes the amplitude of the Johnson noise voltage as a Gaussian distribution [7]. In an ideal case, all the resistors in the circuit would be ideal and would be at zero Kelvins; thus, the resistors would contribute no thermal noise to the measurement. In the case of this project, however, the thermal noise input creates a voltage offset at the outputs. For simplicity, Johnson noise is usually considered as a source of white noise, giving it a flat frequency spectrum, and that would theoretically mean it has infinite energy; however, for the realistic representation of Johnson noise, which Nyquist pointed out in [8] it is in general given by

$$v_{noise}(f) = \frac{hf/kT}{e^{hf/kT}-1} \quad (3)$$

where h is Planck's constant $6.62607004 \times 10^{-34}\ m^2\ kg\ s^{-1}$, and f is the frequency in Hertz.

Next, we look at the flicker noise, also called pink noise. Flicker noise is a type of noise with a 1/f power spectral density (the literature often refers to it as 1/f noise), causing a problem in the lower frequency range and causing a voltage drift. The 1/f frequency distribution is a natural phenomenon seen in many real-world scenarios, such as the frequency of large earthquakes occurring or traffic road blockages. However, in the electrical sense, it arises due to impurities in materials used in the circuit, creating resistance fluctuations. Simple modern-day circuits cannot avoid 1/f noise, but they can attenuate it, as in this circuit design using a high-pass filter.

Amplifier noise is the culmination of all the noise generated within an amplifier circuit, or, in this case, an operational amplifier integrated circuit. Section 4 in this report shows the analysis of different operational amplifiers from Linear Technology, Analog Devices, and Texas Instruments to

find the ones with the slightest noise input for the first stage of the circuit. Amplifier noise is most relevant in the first amplification stage of the circuit, according to Frii's formula for noise. Frii's formula for noise voltage for this circuit, which consists of a buffer, a difference amplifier, and an inverting amplifier, is given by

$$v_{noise} = v_{noise} \ + \frac{1}{A_1^2} \times v_{noise2} + \frac{1}{A_1^2 A_2^2} \times v_{noise} \quad (4)$$

where $v_{noise(n)}$ is the respective noise input before each amplifier stage, and A_n is the amplification of each amplifier [9]. Due to this result, a very low noise amplifier is necessary for the first amplification stage of the circuit. In contrast, the rest of the amplifier stages could be more focused on reducing drift and having a flat bandwidth.

Parasitic impedance sources are the final obstacle considered in this report, and the reduction of these impedances is the main point of improvement in this design. Parasitic impedances result from the traces, wires, fills, planes, and vias present in the actual circuit layout; it is a consequence of the finite resistance, capacitance, and inductance present in every piece of a conductor. Crosstalk between nearby traces also causes a deviation in the measurement, and so the designer takes great care to reduce the input crosstalk and the parasitic impedances.

3. Component Selection

The block diagram for the circuit can be seen in Figure 1 and is a replica of the design seen in [5], but with minor adjustments and additions. It comprises an incandescent lightbulb connected to a power source, a photodiode, an instrumentation amplifier, an inverting amplifier, a low pass filter, an optional temperature module and an ACD to collect and convert the data. The circuit starts with a small LCR circuit built to stabilize the voltage reaching the incandescent lightbulb; it involves inductors to prevent high-frequency electromagnetic interference, a potentiometer to adjust the output voltage of the lightbulb, and a capacitor to smooth the voltage out. The photons emitted from the lightbulb collide with charge carriers in the photodiode, which creates electron-hole pairs; the electrons then cross the PN junction within the diode, generating a noisy current, the source of the noise being Shot noise. This noisy current passes through a 200 Ω resistor connected in parallel with the photodiode; this allows the resistor to create a voltage difference. The voltage difference then connects to the inputs of a gain only instrumentation amplifier, which amplifies the signal; this is to prevent any additional input noise from being added due to passive filtration components. The ADC measures the voltage V1 after the buffer stage of the instrumentation

amplifier. The photodiode voltage then passes through a high pass filter, removing any DC offsets and flicker noise, leaving only the Shot noise and Johnson noise. The amplified signal then passes through a gain inverting amplifier, which also acts as a Butterworth filter; finally, going through an averaging low pass filter with an ample time constant, this averaged Shot noise voltage V2 is then measured and used. The photocurrent is measured at two points in the circuit by a 32-bit ADC, then transferred to a microcontroller via an SPI protocol where it will be processed and put through the circuit's transfer function to yield the measured and calculated charge of the electron. The circuit will be using 1% tolerance resistors to ensure an accurate calculation; the circuit's capacitors will be of electrolytic and tantalum type; this is to prevent any electro piezo noise that any mechanical vibrations of ceramic capacitors would induce.

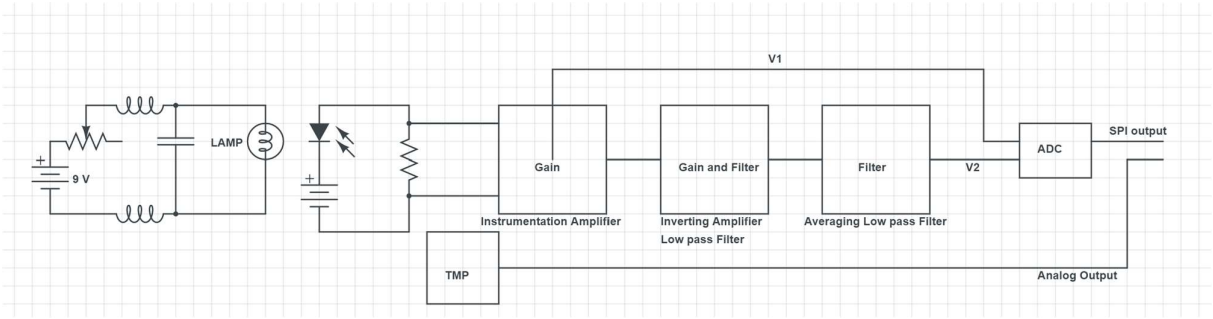

Figure 1 – Block diagram of the design in [5] showing the different blocks the signal will go through before being measured and processed. The circuit starts with a regulated adjustable power stage to generate a noisy light current in the photodiode. The noisy current gets converted into a noisy voltage which is then amplified and filtered and then measured at two separate blocks in the circuit; the measured voltages are in the block diagram as V1 and V2.

The design uses a BPW34 [10] low capacitance photodiode; this photodiode when plugged in reverse bias, can generate a light current of between 2 µA and 50 µA given an irradiance ranging from 0.05 $mW\ cm^{-2}$ to 1 $mW\ cm^{-2}$, its reverse bias current is not affected much by the reverse bias voltage, and so a 3 V battery will suffice to power the diode. The RMS Shot noise current of the photodiode can be given by

$$i_{rms} = \sqrt{2qIB} \tag{5}$$

Where q is the defined charge of the electron $1.602176634 \times 10^{-19}\ C$, I is the photocurrent generated, and B is the bandwidth under consideration [11]. The original design achieves a bandwidth of 100 kHz. That is the desired bandwidth for any improvements in the design. If the

photocurrent generated by the diode is 2 μA, and we take charge of the electron to be its defined value, then, with a bandwidth of 100 kHz, we obtain

$$i_{rms} = 0.253\ nA$$

The circuit connects this noise current to the terminals of a resistor of 200 Ω magnitude, creating a voltage drop, and therefore, we obtain a noise voltage of

$$e_{rms} = i_{rms} \times R = 50.64\ nV$$

With a minimum noise voltage this small, we need amplification of at least 120 dB to achieve an RMS noise voltage in the millivolts range to get a meaningful reading. This small voltage also means that we need our first amplification stage to have an input noise voltage of 50.64 nV or less to achieve a signal to noise ratio (SNR) of 1 or larger.

The original design seen in [5] uses an ADA4898-2 operational amplifier [12] for all the amplification stages; this amplifier provided excellent performance, which resulted in an accurate measurement of just 1% deviation; in an attempt to improve the measurement, this section tests the ADA4898-2 against alternative operational amplifiers. The programmer performs the tests in LTSpice XVII, where the original circuit is designed and put through a noise simulation and an AC analysis simulation. The components are simulated within the completed circuit rather than in small test circuits; this is to see how it would perform through all the gain stages. The programmer tests the original design against several designs with the same format but with slightly different components to find the component with the flattest passband, the lowest input noise voltage spectral density, and the amplification and bandwidth requirements.

The AC frequency simulations test the circuit in the frequency range of 1 Hz up to 100 MHz; the passband to aim for is in the range of 100 Hz to 100 kHz, resulting in the desired 100 kHz bandwidth. The software measures the circuit gain at the 1 kHz frequency for each circuit; the software then compares the gains to see which component provides the best gain with the slightest input noise.

3.1. Instrumentation Amplifier Stage

The first idea was to test out instrumentation amplifier integrated circuits (IC) rather than manually building it using three different amplifiers. The theory uses instrumentation amplifier ICs to reduce the stray impedances present in long copper traces that would connect the three

regular operational amplifiers. Instead, it replaces the copper traces with microscopic traces within the IC. The instrumentation amplifier ICs that had the best noise voltage spectral densities according to their datasheets are the AD8421 [13], the AD8428 [14], and the AD8429 [15]. Table 1 displays a comparison of the mentioned ICs; the table compares their advertised CMRR, gain method, input noise voltage, bandwidth, and offset drift. Figure 2 shows the LTSpice software circuit with the circuit designs. Figure 3 (a)-(d) shows the input noise voltage analysis and AC frequency response for each amplifier.

Table 1 – The AD8421, AD8428, and AD8429 instrumentation amplifiers are compared based on their datasheet's CMRR, input noise voltage, bandwidth, offset drift, and their gain method.

	CMRR (dB min)	**Input noise voltage (nV/√Hz)**	**Bandwidth (MHz) (G=1)**	**Offset drift (µV/°C)**	**Gain method**
AD8421	94	3.2	10	0.2	Resistor
AD8428	130	1.5	3.5	1	Fixed (2000)
AD8429	90	1	15	1	Resistor

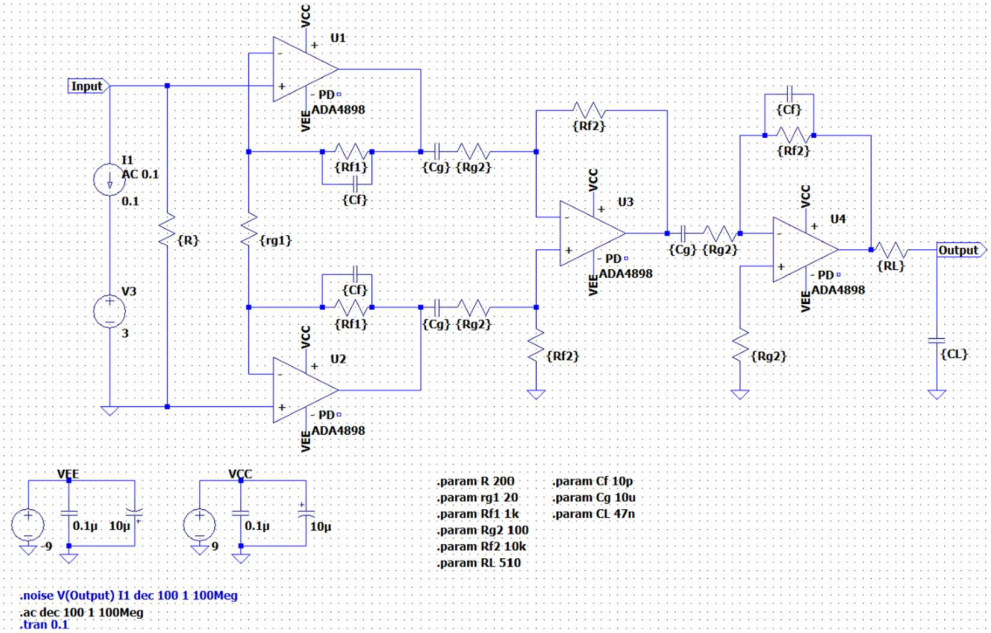

(a)

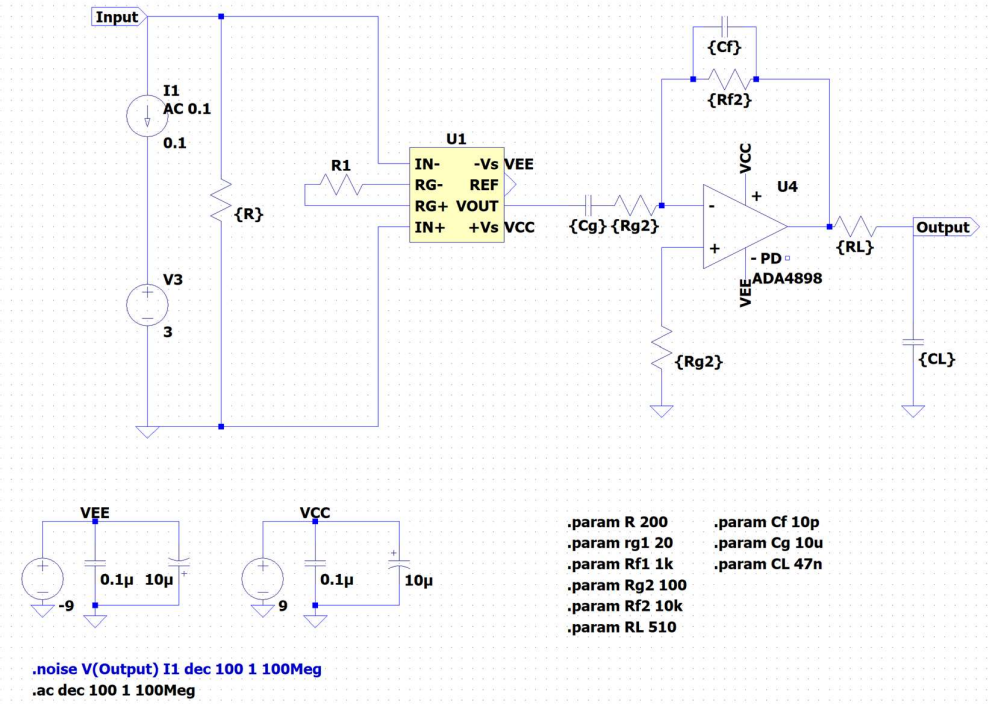

(b)

Figure 2 – The circuit designed in [5] recreated using LTSPICE XVII (a) shows the original circuit with the ADA4898 in place as the circuit's main op-amp. (b) shows the same circuit but with the instrumentation amplifier replace by a single instrumentation amplifier IC. the parameters in (b) differ based on the tested IC requirements.

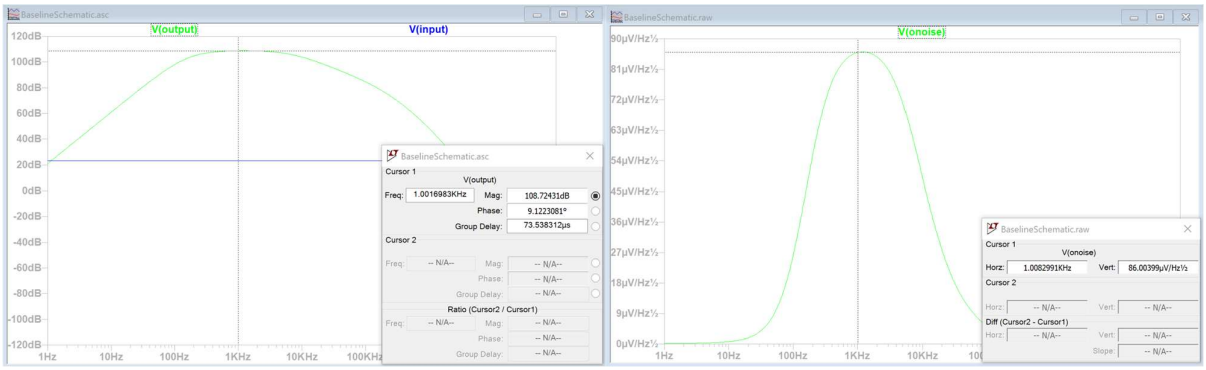

(a)

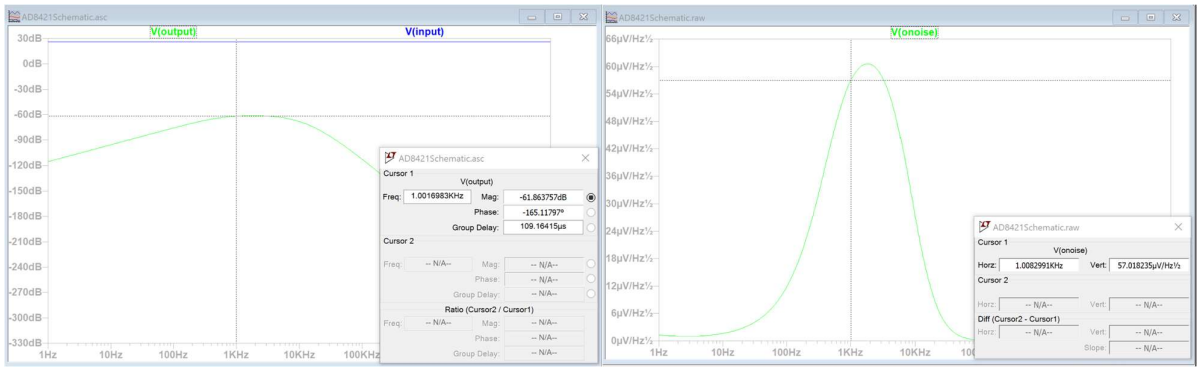

(b)

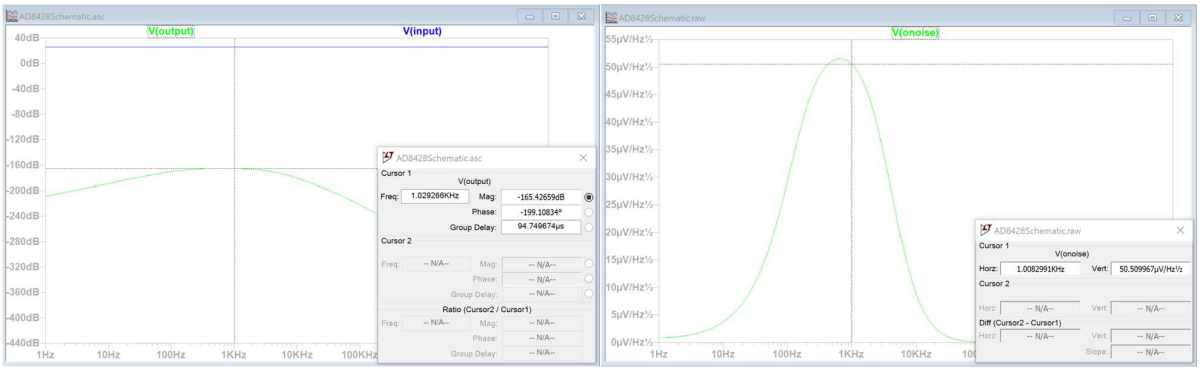

(c)

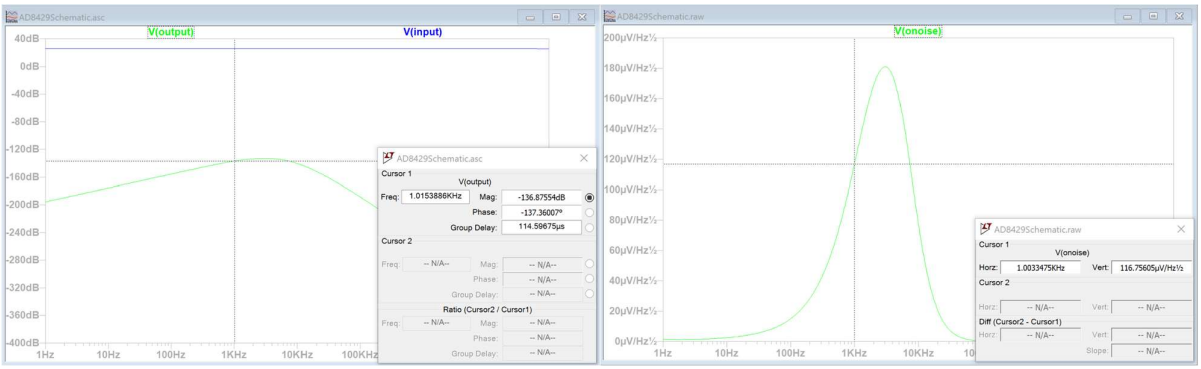

(d)

Figure 3 – Output noise voltage and frequency response simulation results for the (a) ADA4898, (b) AD8421, (c) AD8428, and (d) AD8429. The graphs highlight the total gain in dB (left) and output noise in nV/√Hz (right) at the 1 kHz mark for each of the components tested.

The original design showcased in figure 2 (a) has an output gain calculated using the equation

$$A = \left(\frac{Rf1+{}^{rg1}/_{2}}{{}^{rg1}/_{2}}\right)\left(\frac{Rf2}{Rg2}\right)^{2} \quad (6)$$

using the resistor values in the figure, and in an ideal scenario, we end up with an amplification value of 1010000 (120 dB). However, as seen in Figure 3 (a), the simulation results show amplification of 108.7 dB at the 1 kHz frequency; this is well within the passband. This amplification results in an output noise voltage of 86 μV/Hz$^{1/2}$ at 1 kHz; this section compares these baseline results against all other simulation results.

Figure 2 (b) uses the AD8421 as the instrumentation amplifier; the amplifier's datasheet states that the user can calculate the gain of the AD8421 using the formula

$$1 + \frac{9900}{RG} \quad (7)$$

where RG is the resistor value across the component's RG pins. In this case, the aim is to match this amplifier's gain value to the baseline amplifier's gain of 120 dB; to theoretically achieve this gain, the design is fitted with an RG value of 99 Ohms to give it a gain 101, after that, the programmer adjusts the inverting amplifier's resistor values using the equation for the inverting amplifier

$$A_3 = \frac{Rf2}{Rg2} \quad (8)$$

to achieve a gain of 10,000, which should theoretically result in a total gain of 1010000 (120 dB). The simulation in Figure 3 (b) shows otherwise and shows a gain of -61.8 dB at the 1KHz pass band mark. This simulation result does not compare well with the baseline results. This design would require the addition of multiple extra amplifier stages to reach the same gain; the instrumentation amplifier also displays a large output noise voltage relative to its amplification value.

Next is the circuit with the AD4828 in place, with its simulation results shown in Figure 3 (c). This instrumentation amplifier has a fixed gain of 2000, which is adjustable by connecting a resistor across the "FIL" pins of the amplifier (the RG pins in Figure 2 (b)); the user can calculate the gain using the formula

$$G = \frac{2000 \times RG}{RG+6000} \quad (9)$$

where RG is the resistor between the "FIL" pins. Otherwise, the user can choose a gain and calculate the required resistance by rearranging the formula to

$$RG = \frac{6000 \times G}{2000-} \quad (10)$$

In this simulation, the chosen value for RG is zero, and so a fixed gain of 2000 was maintained. However, the next stage would have a gain of 505 to achieve a total gain of 120 dB; appropriate inverting amplifier resistors were chosen following equation (8) to achieve this gain. The simulation shows a result that does not match the theory; the circuit had a total gain of -165 dB instead of the desired 120 dB, so this component failed to outperform the baseline results. The simulation has also displayed an impoverished output noise voltage relative to its amplification, as seen in Figure 3 (c).

The final instrumentation amplifier IC tested was the AD4829, with its simulation results seen in Figure 3 (d); this amplifier is like the AD8421 in how the user can calculate its amplification value; its gain equation is

$$G = 1 + \frac{6000}{RG} \quad (11)$$

where RG is the resistor across the component's RG pins. This amplifier circuit had the same adjustments as the first test, except RG was chosen to have a value of 60 to account for its internal differences. The theoretical gain of the circuit is 120 dB; however, it showed a gain of -136 dB; it also displayed the most significant input voltage noise despite not having the largest gain among the three tested.

We conclude that using an instrumentation amplifier IC would require drastic changes to the circuit design due to the instrumentation amplifier IC's limited gain and flexibility. Rather than acting like cascaded amplifiers amplified at each stage, The ICs act as a single fixed amplifier with minimal amplification, slightly adjustable with the resistor connected between its unique pins. Additional amplification stages would be needed to allow the instrumentation amplifier to work, which would bump up the price of the circuit and increase the complexity of the equations and the variability of the outcomes.

An instrumentation amplifier IC is not the only solution for improving the first amplification stage; tests replacing the ADA4898-2 with other amplifiers while keeping the same circuit was conducted. The amplifiers chosen for testing were the AD797 [16], LT1115 [17], LT1128 [18], and the LT6200 [19] and Table 2 compares these amplifiers' characteristics. The paper includes the LM741 [20] op-amp circuit as a bonus test to see if the circuit can be as easily accessible as

possible and making it as cheap as possible—figure 4 displays operational amplifier simulation results.

Table 2 – The ADA4898, AD797, LT1115, LT1128, LT6200, and LM741 operational amplifiers are compared based on their datasheet's CMRR, input noise voltage, bandwidth, and their offset drift.

	CMRR (dB min)	Input noise voltage (nV/√Hz)	Bandwidth (MHz)	Offset drift (µV/°C)
ADA4898	120	0.9	65	1
AD797	130	0.9	110	0.2
LT1115	123	0.9	70	0.5
LT1128	126	0.85	75	0.2
LT6200	90	1.5	145	2.5
LM741	95	-	1.5	15

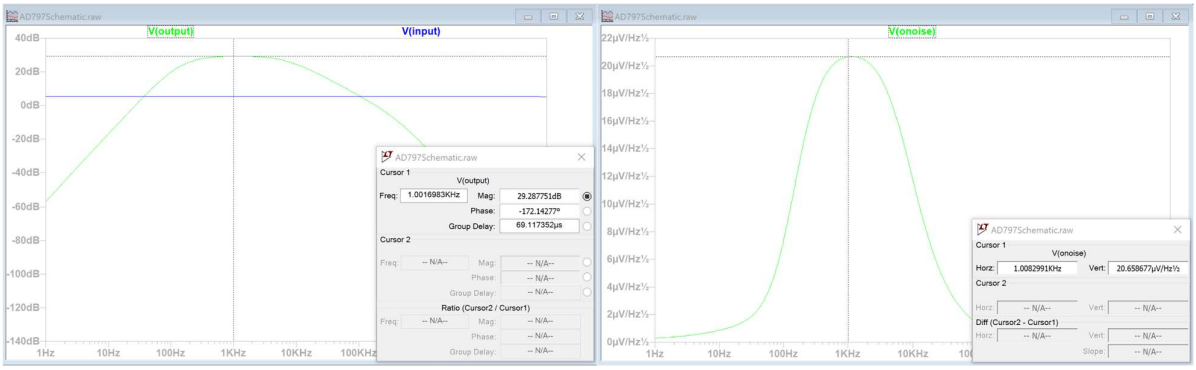

(a)

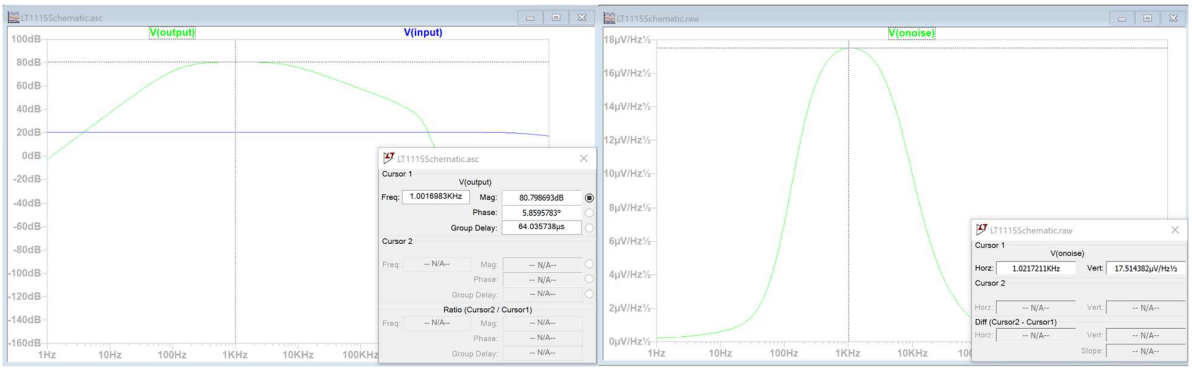

(b)

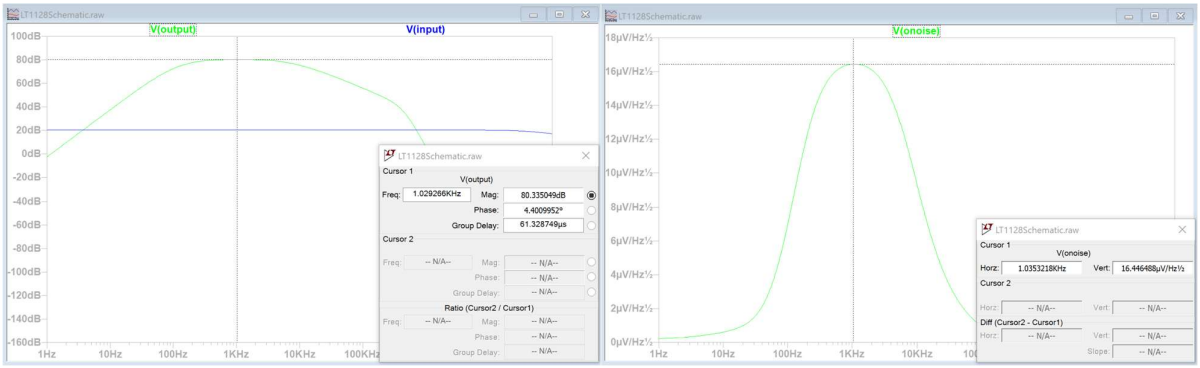

(c)

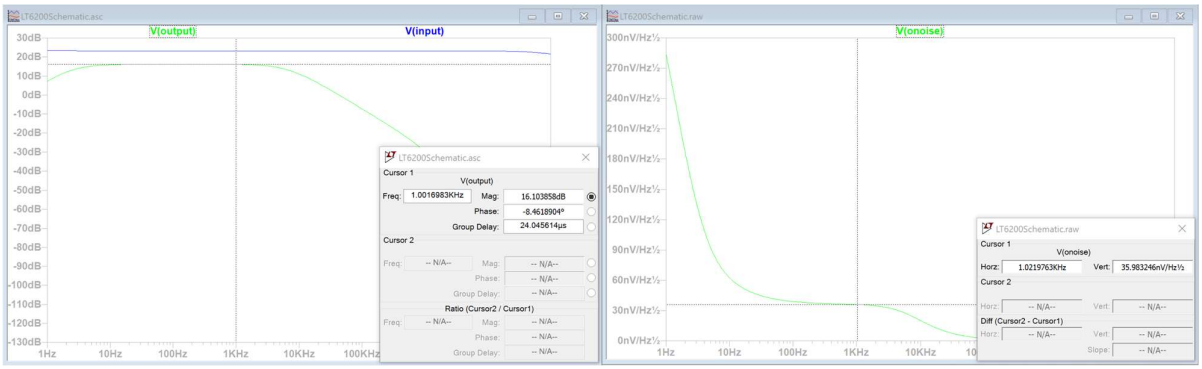

(d)

Figure 4 – Output noise voltage and frequency response simulation results for the (a) AD797, (b) LT1115, (c) LT1128, and (d) LT6200. The graphs highlight the total gain in dB (left) and output noise in nV/√Hz (right) at the 1 kHz mark for each of the components tested.

Figure 2 (a) and Figure 4 (a) showcase the design and simulation using the AD797 operational amplifier as an instrumentation amplifier; the design adjusted the original circuit to have an amplification of 10010000 (140 dB) in contrast to the baseline design's 120 dB. However, the

simulation shows that it only managed to reach a gain of 29 dB at its passband. The operational amplifier does, however, show better noise performance than that of the ICs. It has a better noise performance than the baseline design's noise, but that is due to its smaller amplification value. Next is the LT1115 operational amplifier circuit; this circuit design has a total theoretical amplification of 140 dB, yet it only manages to reach 80 dB amplification. Figure 4 (b) shows the amplifier circuit's output noise. This amplifier performs better than the AD797 amplifier in that it has a more significant amplification, and it has a smaller output voltage noise density. The LT1115 compares very well against the ADA4898. The LT1128 simulated in Figure 4 (c) shows similar results to the LT1115; they both achieve amplification of 80 dB at the passband and have a low input noise voltage nearly one-fifth of the baseline. A more complex operational amplifier design, namely the LT6200, was tested and shown in Figure 4 (d); this amplifier performed poorly in amplifying the desired passband. The achieved gain of this amplifier is 16 dB, smaller than the input signal of the circuit; the LT6200 did, however, display the best output noise voltage among all the amplifiers tested; the small voltage gain of the circuit is the reason for the reduced noise voltage.

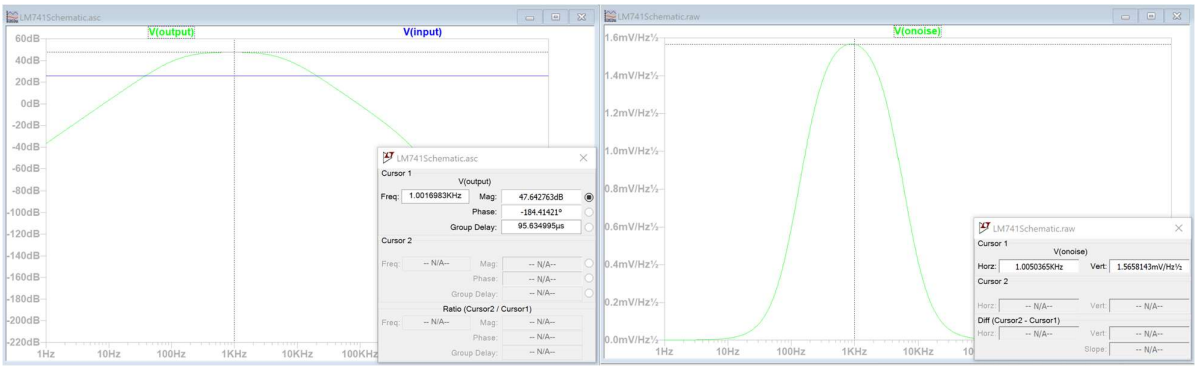

Figure 5 – Output noise voltage and frequency response simulation results for the LM741 operational amplifier. The graphs highlight the total gain in dB (left) and output noise in nV/√Hz (right) at the 1 kHz mark for each of the components tested.

The last amplifier tested is the common LM741 amplifier; Figure 5 displays its simulation results. The figure shows a small gain of 47.6 dB, despite having a theoretical gain of 120 dB; the component also introduces a tremendous output voltage noise within the passband frequencies. The simulation shown in Figure 5 is the expected result. The designers did not make this component for precision applications; it can still be used for simple, less precise tests using breadboard and jumper wires and achieve reasonable accuracy.

With all this data available, The work concludes that the best operational amplifier tested remains the ADA4898; this is due to its ability to achieve a significant gain close to the desired theoretical gain while maintaining the desired passband for the circuit. Another advantage of this amplifier is that it offers a dual package that keeps components close together and reduces the parasitic noise.

The transfer function for the amplifier buffer stage is

$$A_1 = \frac{Rf1 + {}^{rg1}/_{2}}{{}^{rg1}/_{2}} \tag{12}$$

And the difference amplifier stage

$$A_2 = \frac{Rf}{Rg2} \tag{13}$$

3.2. Inverting Amplifier and Filtration

This stage of the circuit uses an inverting amplifier that also acts as a Butterworth filter. Considering the last high-pass filter in the circuit appears before the inverting amplifier stage, an attempt to improve the design is to have a minimum voltage drift generate in this stage. Analog Devices offers the ADA4528 [21] as their low noise operational amplifier with the smallest offset drift voltage. The ADA4528 advertises a maximum offset voltage of 2.5 µV compared to the ADA4898, which has a maximum drift of 160 µV. Figure 6 shows the result of the circuit simulated in LTSpice XVII with the inverting amplifier stage component replaced with the ADA4528 to minimize the voltage offset.

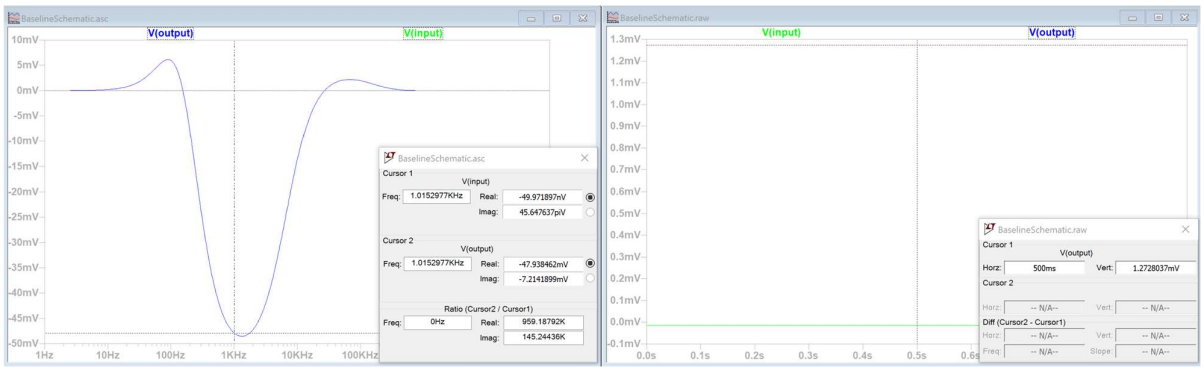

(a)

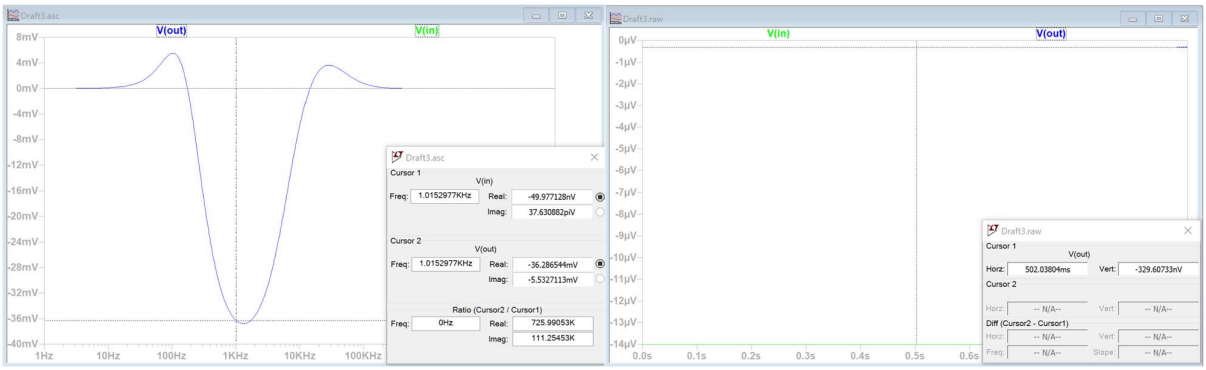

(b)

Figure 6 – Simulation results with the (a) ADA4898 and (b) ADA4528 operational amplifiers used in the inverting amplifier stage. Left shows the frequency response of the complete circuit, and right shows the circuit's transient response with no input voltage.

Figure 6 shows that the ADA4528 outperforms the ADA4898 when it comes to reducing the offset current created; however, this comes at the cost of reducing the circuit's bandwidth by half and reducing the gain slightly. Nonetheless, the ADA4528 will be used instead of the ADA4898 for its reduced offset voltage.

3.3. Extra Components

The new design will use roughly the same components to adjust to the inverting amplifier made earlier. Additionally, the circuit will include an ADC to make the two voltage measurements V1 and V2. Considering that precision is a critical element in the design, a low noise ADC is required; the bit range of the ADC, a 32-bit ADC, provides the best precision. This subsection studies the two highest resolution and cheapest ADCs offered by Analog Devices; an AD7177-2 [22], costing $14.65, and an LTC2508-32 [23], costing $8.95. Looking through the datasheets, we note that the AD7177-2 offers five analogue input channels, meaning the circuit can directly connect voltage sources to the ADC; however, that is the only advantage that it has over the LTC2508-32 in this situation. The LTC2508-32 offers a single low noise analogue input and two SPI protocol digital outputs, one of which outputs 32-bit data and the other outputs 22-bit data. This device has 25 pins, 12 of which are digital and considered in the software implementation. The 12 pins on the left of the device are mainly power pins and the analogue voltage input; the circuit connects this voltage input to an additional component, a simple switch that will connect to the two measured voltages and switch between them.

4. PCB Implementation

4.1. Layout Design

A theoretical design of a circuit schematic is just a show of the netlist present in the circuit and does not say anything about how it would behave in the physical world; hence, the need for a good layout design. The original work has a simple layout designed for the circuit where the components are maintained in proximity by choosing dual op-amp IC. The layout has a few large loop areas, which was unavoidable considering the designer used a single layer PCB.

Implemented here is a two-layered PBC; this provides better routing opportunities for the components and mitigates the loss of changing from a dual op-amp to two separate op-amps. The Altium 21 is the software used to design the circuit; Appendix 1 contains the schematic representation of the block diagram seen in Figure 1 and all the required component values. Appendix 1 also displays the detailed layout for the schematic, with its three-dimensional view shown in Figure 7.

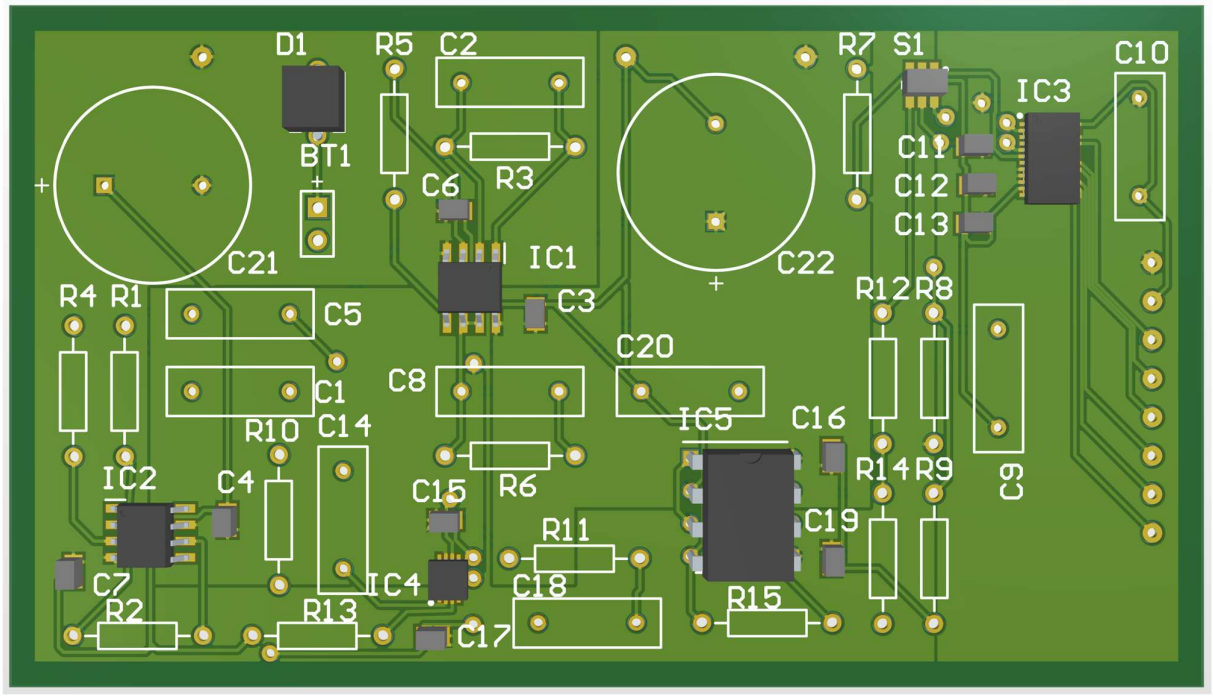

Figure 7 – Three-dimensional representation of the circuit design with an ADC and Analog multiplier included.

This schematic is a replica of that in [5]; this schematic adds a switch and connects it to the V1 and V2 outputs; this switch then connects to the ADC's analogue inputs, where the voltages are

measured and turned into 32-bit digital data to be processed by an externally connected microcontroller. The original work did not make much use of the board space with their layout; this section presents a new suggested layout to improve the design theoretically. This layout has the bottom layer entirely dedicated to the ground net, except for a few vias and traces; this reduces the impedance of the return currents by allowing the current to take the path of most negligible impedance. The layout has the top layer split into three power polygons, with traces and vias connecting the components. There is a rectangular 3.3 V power polygon encompassing the ADC and powering most of its inputs to the board's right. A microcontroller's 3.3 V power output powers this net. A -9 V VEE power polygon directly connects to all VEE IC power inputs and decoupling capacitors on the left side of the layout. The VEE polygon is another smaller polygon within the 9 V VCC polygon; this encompasses all VCC power inputs and decoupling capacitors. The large power surfaces present in the layout create capacitance between the copper polygons; This capacitance helps store charges and counteracts the inductive impedances caused by higher frequency components within the signal.

The layout takes care to ensure that power inputs are connected close by their respective polygons and decoupling capacitors close to their power inputs. The design follows the guidelines of the ADC's datasheet with the magnitudes and positioning of its decoupling capacitors. The circuit has its ground net referenced by the battery midpoint and the ground output pin of the connected microcontroller.

4.2. Experiment

When running the experiment, the user must construct a separate breadboard circuit; this breadboard circuit will comprise a couple of batteries, two inductors, a capacitor, a potentiometer, and an incandescent lightbulb. The original work further elaborates on this circuit stage. The user should connect two 9 V batteries between the three empty vias found at the top of the layout to power the central part of the board. The board's right provides eight empty vias meant to connect to a microcontroller using jumper wires; the vias, from top to bottom, are connected to the ADC's OVDD GND, BUSY, SCKA, SDOA, DRL, SYNC, and MCLK pins. The mentioned pins provide the ADC's digital functionality and are explored later in this paper. Figure 8 shows a block diagram for setup.

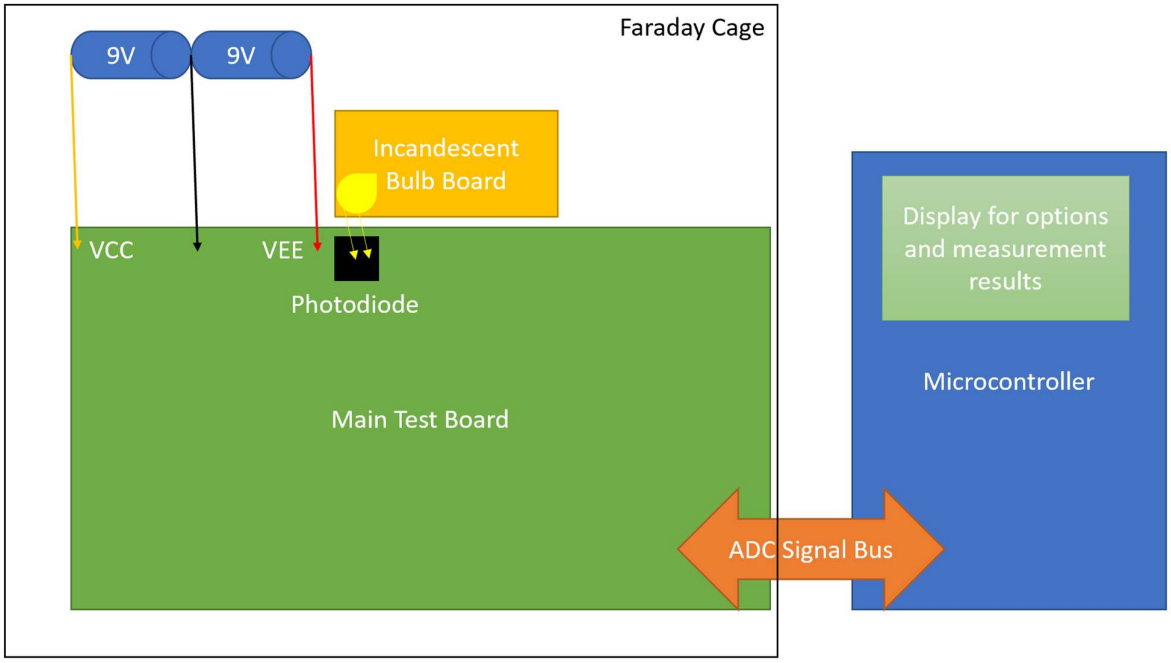

Figure 8 – A block diagram showing the required connections for the experiment setup.

With everything set up, the user should place the circuit in a refrigerator or any other form of a faraday cage, such as a box covered with aluminium foil or a dryer. As stated earlier in the paper, this will reduce the electromagnetic interference that the circuit experiences. A suitable case is a cookie box with holes drilled to allow wiring to pass through; the experimenter can wrap the cookie box with aluminium foil or ferrite sheets. If the user places the circuit in a refrigerator, the components' temperatures will reduce, reducing the amplifier noise and the Johnson noise. After preparing the setup, the user should measure all the resistor and capacitor values using the lab's multimeter; these values may differ due to the small variability factor of real components and the variability due to temperature. The circuit should take the first measurement of V1 after the averaging filter's time constant time before flipping the switch S1 to measure the voltage V2. The user then turns the potentiometer to increase the incident photons on the photodiode and then repeat the steps until the microcontroller has gathered sufficient data. The microcontroller can then go on and calculate the charge of the electron with the measured data.

5. Final Equation and Software

An equation can be derived now with the component selection sorted and the layout design implemented, with the guidance of [5] by combining the transfer functions for the different sections of the circuit and using the noise analysis mentioned earlier.

5.1. Derivation

The equation calculating the electron charge derived in [5] is present here; the equation is

$$q_e = \frac{2rg1}{Rf1+}\left(\frac{Rg2}{Rf2}\right)^4 \frac{U_m}{R}\frac{R1}{R1+R2}\frac{Rv+Rav}{ZRv}\frac{\Delta V2}{\Delta V1}\frac{4}{B} \quad (14)$$

B is the total bandwidth of the circuit measured in Hz. The original work only considers the bandwidth of the last low-pass filter before the analogue multiplier. Here we will derive the actual bandwidth for all stages of the circuit.

The first stage of the circuit is the buffer amplifier; this amplifier is set up as an active low-pass amplifying filter to amplify and average the original photovoltage V1. The amplifier setup's transfer function is

$$G_1 = \frac{A_1}{1+s\times Rf1\times Cf} \quad (15)$$

After the active low-pass filter comes to a passive low pass filter, with the transfer function

$$G_2 = \frac{s}{s+\frac{1}{Rg2\times Cg}} \quad (16)$$

The next stage in the circuit is the difference amplifier, which provides no filtration and amplifies the differential input signal. Another high-pass filter placed afterwards attenuates the intrinsic flicker noise and removes the voltage offset generated by the amplifier; to calculate this filter's transfer function, we also use equation (16). The inverting amplifier also has the setup of an active low-pass amplifying filter, with its transfer function being

$$G_3 = \frac{A_3}{1+s\times Rf2\times Cf} \quad (17)$$

Finally, is a passive low-pass filter, this filter's transfer function is given by

$$G_4 = \frac{1}{1+s\times RL\times CL} \quad (18)$$

A convolution operation between all the transfer function stages is present to calculate the total bandwidth of the system; since all the transfer functions are in the frequency domain, the convolution is just a matter of multiplication. The convolution does not include the amplifier gains A_1 and A_3 as those are already present in equation (14). The result of the convolution is as follows

$$G_{total} = G_1G_2G_2G_3G_4 = \frac{as^2}{bs^5+cs^4+ds^3+fs^2+gs+1} \quad (19)$$

The convolution results in a long algebraic fifth-order bandpass filter equation representing the whole circuit; the experimenter can shorten the equation by adding the measured resistor and capacitor values. Using a simple online algebraic equation calculator, the user can perform the multiplication with the measured values. The total system transfer function is then integrated throughout its full spectrum to give the total bandwidth of the system

$$B = \int_0^\infty |G_{total}| \frac{ds}{2\pi} \quad (20)$$

After measuring the resistor values, the user can compute this definite integral using an online integral calculator or manually perform the calculation; the user can confirm this calculated value by comparing it with the circuit's frequency response measured by an oscilloscope. Equation (14), with all the measured resistor values and with the new bandwidth derivation, can now be implemented in software.

5.2. Software Calculation

When the microcontroller initiates the software, the ADC will begin its systematic data collection; the ADC will measure the analogue voltages in the V1 and V2 nodes and convert them into digital signals. The ADC outputs its digital data in a Serial Peripheral Interface (SPI) protocol wrapper; this data is output through the ADC's SDOA pin, which should connect to a microcontroller pin capable of receiving SPI inputs. The SPI input is then converted from 32-bit data to a floating-point variable using the equation

$$V_{Bit} = \frac{2 \times V_{REF}}{2^{32}} \quad (21)$$

This equation gives the data a resolution of V_{Bit}; The datasheet [23] states that the output data is in 2's complement format. The microcontroller will connect its peripheral clock to any of its compatible GPIO pins and connect that pin to the measurement board's MCLK pin; another GPIO pin sends an output clock signal connected to the SCKA pin. The rising edge of the SCKA clock controls the rate at which data is output from the SDOA pin. The microcontroller will read the measurement board's BUSY and DRL pins to know whether the data is ready; it will output the appropriate signal to the SCKA pin when data is ready.

The ADC uses a downsampling factor of 256 because the calculation does not require plenty of

measurement samples; This configuration is done by connecting the SEL0 and SEL1 pins to the ground reference. The SYNC pin is helpful if multiple measurement boards are used and connected to the same microcontroller; it synchronizes the data outputs of the different measurement boards.

The Appendix 2 section of this paper has a pseudo-code software that the user can convert and implement using the preferred language and preferred microcontroller.

6. Conclusion

This report is merely a theoretical improvement to the original work done in [5]; it serves as a review of the design with several suggested alterations to the original work. The goal was to achieve high accuracy while keeping a low price for the circuit. The price for the circuit has more significant due to using a two-layer PCB rather than a single layer. However, the addition of a PCB layer theoretically comes with an improvement in accuracy and power dissipation and should be worth the minor extra charges.

This paper showcased several components' tests, all of which failed to outperform the ADA4898-2 in all its amplification stages, except for the ADA4528, which outperformed it in its input drift the final inverting amplifier stage. The changes made to the circuit are as follows, a single component change, an addition of an ADC to measure the voltage outputs, the addition of pins to read and write to and from the ADC using a microcontroller, an improved layout design, some minor changes to the original work's final equation, and the addition of pseudo-code software capable of performing the necessary calculations.

This PCB can be mass-produced and sold to high schools, where it can act as a fun lab exercise that gives secondary school students an intuition of how the electron charge they learn about can be measured. This experiment teaches the electron to students using a more modern and applicable method rather than sticking to Millikan's twentieth-century oil drop experiment. It could also serve as a first-year undergraduate guided project, giving the students an intro to precision electronics and intuition on the electron charge origins.

Finally, a couple of suggested improvements to the design; the PBC could be printed and physically tested to see where it is lacking or where there are additional noise sources and whether an ADC does more harm than good. Later in the future, newer, very low noise amplifier component models can be added and compared to those used in this design and different low noise ADCs.

7. References

[1] Nobel Foundation, Nobel Lectures Physics, Amsterdam - London - New York: Elsevier Publishing Company, 1965.

[2] I. Bishop, S. Xian and S. Feller, "Robert A. Millikan and the Oil Drop Experiment," *American Association of Physics Teachers,* vol. 57, p. 442, 2019.

[3] The NIST Reference on Constants, Units, and Uncertainty, "physics.nist.gov," CODATA, 2018. [Online]. Available: https://physics.nist.gov/cgi-bin/cuu/Value?e. [Accessed 20 03 2021].

[4] Consultative Committees of the CIPM, "Information for users about the redefinition of the SI," in *Bureau International des Poids et Mesures*, 2019.

[5] T. M. Mishonov, E. G. Petkov, N. Z. Mihailova, A. A. Stefanov, I. M. Dimitrova, V. N. Gourev, N. S. Serafimov, V. I. Danchev and A. M. Varonov, "Simple do-it-yourself experimental set-up for electron charge qe measurement," *Physics.ed-ph,* 2018.

[6] F. Rice, "A Frequency-Domain Derivation of Shot-Noise," *American Journal of Physics,* vol. 44, no. 84, 2016.

[7] P. Horowitz and W. Hill, "Low-Noise Techniques," in *The Art of Electronics*, New York, Cambridge University Press, 2015, p. 506.

[8] H. Nyquist, "Thermal Agitation of Electric Charge in Conductors," *American Physical Society,* vol. 32, no. 1, p. 110, 1928.

[9] Wikipedia, "Friis formulas for noise," Wikipedia The Free Encyclopedia, 04 07 2020. [Online]. Available: https://en.wikipedia.org/wiki/Friis_formulas_for_noise#:~:text=Friis%20formula%20or%20Friis%27s%20formula,ratio%20of%20a%20multistage%20amplifier.. [Accessed 28 03 2021].

[10] Vishay, *Silicon PIN Photodiode.*

[11] P. Cristofolonini, “Shot and Thermal Noise,” [Online]. Available: https://web.archive.org/web/20181024162550/http://www.fis.unipr.it/~gigi/dida/strumentazione/harvard_noise.pdf. [Accessed 15 04 2021].

[12] Analog Devices, *High Voltage, Low Noise, Low Distortion, Unity-Gain Stable, High Speed Op Amp,* 2015.

[13] Analog Devices, *3 nV/root-Hz, Low Power Instrumentation Amplifier,* 2020.

[14] Analog Devices, *Low Noise, Low Gain Drift, G = 2000 Instrumentation Amplifier,* 2012.

[15] Analog Devices, *1 nV/root(Hz) Low Noise Instrumentation Amplifier,* 2017.

[16] Analog Devices, *Ultralow Distortion, Ultralow Noise Op Amp,* 2015.

[17] Linear Technology, *Ultralow Noise, Low Distortion, Audio Op Amp.*

[18] Linear Technology, *Ultralow Noise Precision High Speed Op Amp.*

[19] Linear Technology, *165Mhz Rail-to-Rail Input and Output, 0.9nV/root(Hz) Low Noise, Op Amp Family.*

[20] Texas Instruments, *LM741 Operational Amplifier.*

[21] Analog Devices, *Precision, Ultralow noise, RRIO, Zero-Drift Op Amp,* 2017.

[22] Analog Devices, *32-bit, 10 kSPS, Sigma-Delta ADC with 100 us Settling and True Rail-toRail Buffers,* 2016.

[23] Linear Technology, *32-Bit Oversampling ADC with Configurable Digital Filter,* 2016.

8. Appendices

8.1. Appendix 1

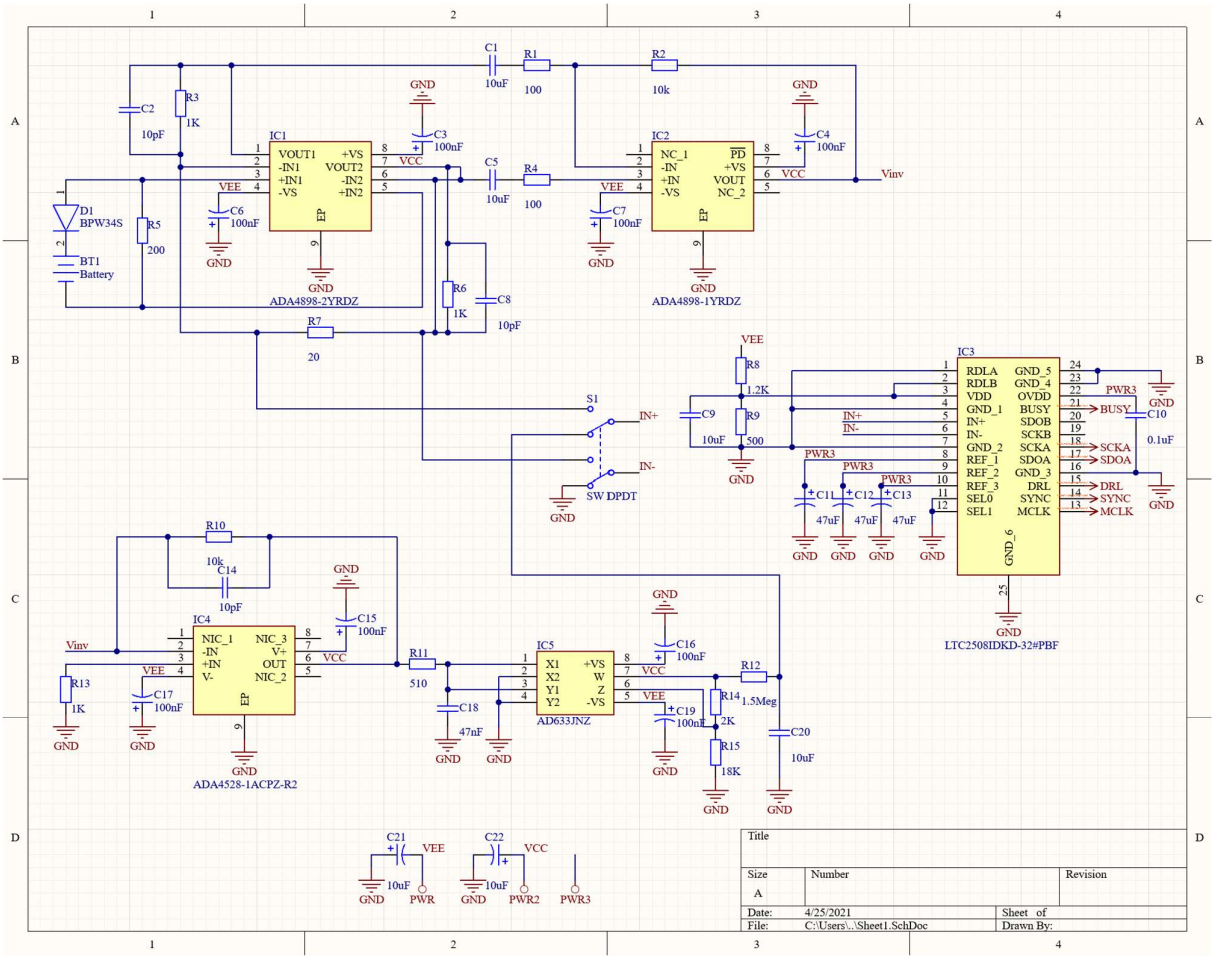

Figure 9 – Altium 21 schematic design for the circuit setup.

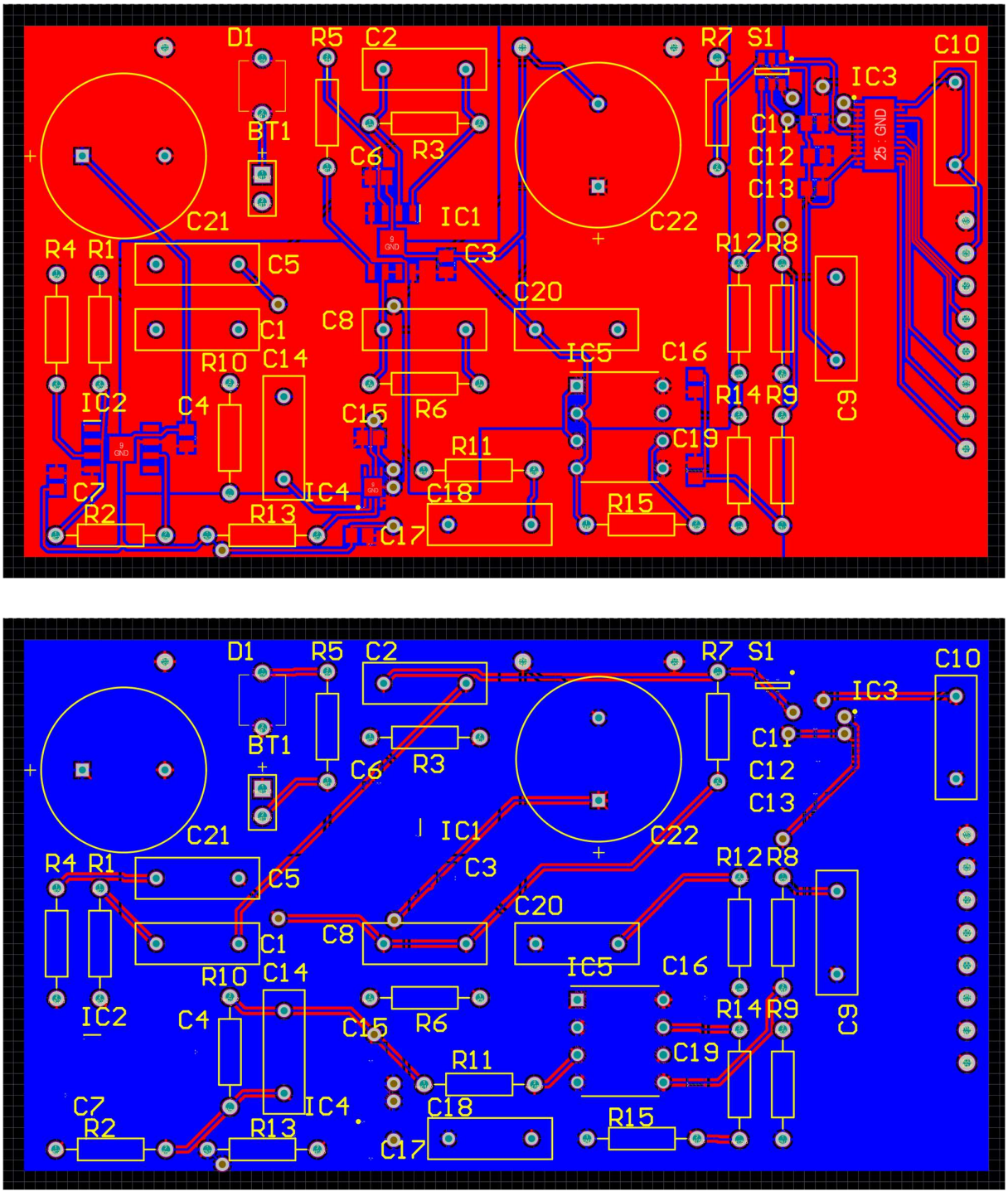

Figure 10 – Altium 21 layout design for the circuit setup; top layer (red) and bottom layer (blue).

8.2. Appendix 2

The microcontroller software's pseudo-code is as follows:

Libraries: Microcontroller's dedicated library

Display screen's library

Definitions: Resistor values

Capacitor values

Z value (given in [5])

GPIO output: Pin A to MCLK – Peripheral clock

Pin B to SCKA – PWM signal at the rate the user desires

GPIO input: Pin C to SDOA – SPI protocol input (store in a 32-bit variable)

Pin D to BUSY – Boolean input (store as a status variable)

Pin E to DRL – Boolean input (use as an interrupt, takes you to ISR)

Functions: ISR – Reads Pin C and stores it

Converter – Use equation (21) to convert SPI to floating point

Slope calculator -

Elementary charge calculator – Performs the complete circuit calculation (the programmer must measure new resistor and capacitor values before every experiment and put them in the definitions before compiling)

The main menu – Uses "switch" or "cascaded if" statements to choose what is on display. A microcontroller button can perform calculations or stop the output clock signal (thus stopping the measurements). With enough measurements, the microcontroller can perform the slope calculation proceeded by the elementary charge calculation.